

Guided image filtering using signal subspace projection

Yong-Qin Zhang^{1,2}, Yu Ding², Jiaying Liu¹, Zongming Guo¹

¹Institute of Computer Science and Technology, Peking University, Beijing 100871, People's Republic of China

²Paul C. Lauterbur Research Centre for Biomedical Imaging, Shenzhen Key Laboratory for MRI, Shenzhen Institutes of Advanced Technology, Chinese Academy of Sciences, Shenzhen 518055, People's Republic of China

E-mail: liujiaying@pku.edu.cn

Abstract: There are various image filtering approaches in computer vision and image processing that are effective for some types of noise, but they invariably make certain assumptions about the properties of the signal and/or noise which lack the generality for diverse image noise reduction. This study describes a novel generalised guided image filtering method with the reference image generated by signal subspace projection (SSP) technique. It adopts refined parallel analysis with Monte Carlo simulations to select the dimensionality of signal subspace in the patch-based noisy images. The noiseless image is reconstructed from the noisy image projected onto the significant eigenimages by component analysis. Training/test image are utilised to determine the relationship between the optimal parameter value and noise deviation that maximises the output peak signal-to-noise ratio (PSNR). The optimal parameters of the proposed algorithm can be automatically selected using noise deviation estimation based on the smallest singular value of the patch-based image by singular value decomposition (SVD). Finally, we present a quantitative and qualitative comparison of the proposed algorithm with the traditional guided filter and other state-of-the-art methods with respect to the choice of the image patch and neighbourhood window sizes.

1 Introduction

Image denoising is still a challenging task in the procedures of image and video processing systems, for example acquisition, processing, coding, storage, transmission, reproduction and printing. Whereas preserving image features such as edges, textures, and details, it refers to the recovery of a digital image that has been contaminated by some types of noise, for example Gaussian noise (AWGN), Rician noise, salt and pepper noise, speckle noise, impulse or Poisson noise. As far as we know, image denoising was first studied by Nahi [1] and Lev *et al.* [2] in 1970s. Then in 1980s, Lee [3] introduced local statistics to study image enhancement and noise filtering. Donoho [4] and Simoncelli and Adelson [5] studied noise removal with wavelet transforms in late 1990s. Subsequently many wavelet-based image denoising algorithms have appeared in these literatures [6–11]. However, these methods often blur fine details and smooth out the edges.

Since the non-local mean (NLM) algorithm by Buades *et al.* [12] has renewed the interest into this classical inverse problem, many more powerful denoising techniques have been proposed in the past several years [13–29]. However, the vast majority of image denoising algorithms have implicit assumptions on signal or attenuation properties, which limits the generality. The NLM algorithm [12] is based on the image spatial self-similarity with better performance than traditional denoising methods, but its similarity measurement between the target pixel and its

associated pixels is related to noise types. The discrete universal denoising (DUDE) method proposed by Weissman *et al.* [14] uses the similarity of the statistical region for text correction, character recognition, and image denoising and achieves good performance, whereas DUDE is less effective to eliminate the additive noise. In addition, it depends on the statistical probability of the pixel's neighbourhood and the signal is limited to discrete values. The unsupervised, information-theoretic, adaptive image filtering (UINTA) in [15] adopted Markov nature of the input image from different contexts to learn the conditional probability density function (PDF) and update the pixel values in order to reduce the randomness. However, UINTA employs information entropy as decision criterion that also damages the details and textures of the image. The TLS-based algorithm proposed by Hirakawa and Parks in [18], needs accurate estimation of noise parameters. The kernel regression (KR) method with recursive iterations proposed by Takeda *et al.* [22] has expensive computation, and is difficult to achieve real-time processing. The denoising algorithm using grey polynomial proposed by Zhang *et al.* [23] can acquire better filtering effect of salt and pepper noise, but has poor results for additive Gaussian noise. The guided filter approach [24] can remove image noise and preserve edges. However, it has poor performance in the low SNR images. It also lacks of reliable approach to optimally select parameters, which seriously affects its practicality. The bilateral filter [21, 25] compares only intensity level values in a single pixel,

which is not robust when these values are corrupted by high level noise. Nevertheless, if the assumptions contained in the denoising techniques cannot be met, such filters will lead to blurred edges and loss of fine structures.

As we know, for a single input noisy image, it is also used as the reference image of guided image filtering method for weight calculation [24, 30]. Inspired by both the Karhunen–Loeve transform (KLT) filter [26] and joint bilateral filter approach [31], we develop a novel algorithm based on local linear minimum mean-square error (LMMSE) predictors to achieve resolution enhancement for noisy images and to improve the preservation of edge sharpness. Comparing to the existing guided filtering technique [24, 30], the proposed method utilises the projection of the patch-based image onto signal subspace determined by improved parallel analysis with Monte Carlo simulation as the reference image. The smallest singular value of the patch-based image matrix is the estimate of the noise standard deviation, and the regularisation parameters are automatically selected by polynomial fitting technique. A comparison of the proposed approach with the state of the arts is also presented.

The rest of this paper is organised as follows. In Section 2, we briefly review the related concepts, and the proposed scheme of single image denoising is described here. Section 3 shows the simulation and experimental results of the proposed algorithm, and the comparison to the state-of-the-arts methods. Finally, we discuss the key findings and conclude our study in Section 4.

2 Proposed algorithm

In real-world digital-imaging devices, the acquired images are often corrupted by device specific noise. Mathematically, the goal of image denoising methods is to recover the clean image from an observed noisy measurement. And the mixed noise model of independent additive and multiplicative types is generally used to describe the noisy image [18]

$$x = s + n_0 + n_1 s \quad (1)$$

where x is the observed image, s is the ideal noiseless image, and n_0 and n_1 represent additive and multiplicative noises, respectively. Many literatures prefer working with an independent additive noise [12, 15, 22], such as Gaussian noise model. That is to say, a simplified noise model instead of (1) denoting the degradation process, is given in the following formula

$$x = s + n_0 \quad (2)$$

Where x and s are defined in (1). Note that (2) is a special case of (1). Although the mathematical elegance and simplicity makes (2) attractive for the complex task of designing a denoising algorithm and describing a natural image, this noise model often requires additional techniques to describe the real-world systems. The image denoising algorithm attempts to obtain the best estimate of s from x . The optimisation criterion can be mean-squared error (MSE)-based or perceptual quality driven, whereas the problem of image quality assessment has not been resolved, especially in the absence of an original reference.

2.1 Formulation of stacked patches

The scene captured in data acquisition or data storage is often a single image or multiple images deteriorated by various noise sources. Consequently, the image denoising has become a key focus of ongoing studies in recent years. Assume that x_i denotes the i th pixel in the observed image $X \in \mathbb{R}^{M \times N}$ and Y is a column stacked patch-based representation of X , that is, Y is a matrix of size $L \times P$ where $L = M \times N$, whose each row contains the $\sqrt{P} \times \sqrt{P}$ patch around the location of x_i in the image X . Moreover, image patch centred at a pixel on the matrix border is padded with mirror copies of the array elements.

2.2 Matrix decomposition of patch-based image

The singular value decomposition (SVD) operator, which transfers a set of correlated variables into a new set of uncorrelated variables, has the interesting properties that they capture the variation of functions defined on the graph from the largest to the smallest singular values. These eigenfunctions form the basis for a real or complex matrix. We find that most of the energy of a function defined on the graph is concentrated at several principal components. Moreover, the eigenfunctions generated from noisy data are able to capture the main characteristics of the corresponding clean signal, whereas the eigenvectors of the smaller singular values are almost all noise.

By removing the mean value from each row, the difference vectorised image from the patch-based image matrix is computed as

$$Z(i, p) = Y(i, p) - \frac{1}{L} \sum_{i=1}^L Y(i, p) \quad (3)$$

where $i = 1, 2, \dots, L$, and $p = 1, 2, \dots, P$.

To reduce computation time, the covariance matrix $Z^T Z$ instead of Z is used to be factorised by this form

$$Z^T Z = U \Sigma^2 U^T \quad (4)$$

where the symbol T denotes the transpose operator, and U is the unitary matrix of eigenvectors derived from $Z^T Z$. Σ is a $P \times P$ diagonal matrix with its singular values $\lambda_1 \geq \lambda_2 \geq \dots \geq \lambda_r \geq 0$ and $r = \text{rank}(Z^T Z)$.

After the projection of Z onto the new basis U , the reformed uncorrelated matrix \hat{Z} is

$$\hat{Z} = Z \times U \quad (5)$$

Therefore the new axes are the eigenvectors of the correlation matrix of the original variables, which capture the similarities of the original variables based on how data samples projected onto them. As we know, if the eigenvalues are very small and the size of image patch from a single noisy image is large enough, the removing eigenmodes of the less significance do not lose much information. From the diagonal singular values, only the first K eigenvectors are chosen based on their eigenvalues. Since the parameter K should be not only large enough enough to allow fitting the characteristics of the data, but also small enough to filter out the non-relevant noise and redundancy. Therefore, the top K largest values are properly selected by PA with Monte Carlo simulation.

2.3 Proposed number of factors to retain

The PA firstly introduced by Horn [32, 33], which in fact is a Monte Carlo simulation technique, compares the observed eigenvalues extracted from the correlation matrix to be analysed with those of an artificial data set obtained from uncorrelated normal variables. This data set is generated by drawing samples from a multivariate normal distribution with the dimensionality P , the same number of observations L , and the same marginal standard deviations as the actual data. Let λ_p for $1 \leq p \leq P$ denote the singular values of the vectorised patch-based image Z sorted in descending order. Similarly, let α_p denote the descendingly sorted singular values of the artificial data matrix. Therefore PA estimates data dimensionality as

$$K = \max\left(\left\{1 \leq p \leq P \mid \lambda_p \geq \alpha_p\right\}\right) \quad (6)$$

The intuition is that α_p is a threshold for λ_p below which the p 'th component is judged to have occurred because of chance. Currently, it is recommended to use the singular value of the artificial data that corresponds to a given percentile, such as the 95th of the distribution of singular values derived from the random data.

In our algorithm, without the assumption of a given random distribution, we generate the artificial data by randomly permuting each element of the neighbourhood vector centered at each pixel. Let $y_{i, p}$ denote the p 'th element of the patch-based neighbourhood vector y_i , centred at pixel position x_i . For each P elements of the vector y_i , a random permutation of the index sequence $p = 1, 2, \dots, P$ is generated by uniform distribution. Thus the mean value, maximum, minimum and random distribution of the artificial data is satisfied for each image patch-based vector.

Then the singular values α of the random artificial data are computed by SVDs which keeps the marginal distributions intact whereas breaking any interdependencies between them. For the L by P synthetic matrix C , after multiple times (e.g. 50) of Monte Carlo simulations, summary statistics (e.g. 95th percentile) can be used to extract the P singular values and order them from largest to smallest. Then PA is applied and the intersection of the two lines denoting singular values of the simulated data C and difference vectorised image Z is the cutoff for determining the number of signal subspace dimensions present in the noisy image. As we know, the noise variance is intimately related with the smallest singular value of simulated data [34]. From the theory and simulation, we found that the singular values of noise matrix are different, which approximately linearly decrease gradually with the dimension. Therefore the increment between the smallest singular value and the largest one from the simulated noise matrix can be used for dimensionality reduction of the noisy image data. The our proposed approach of the corrected singular values of the artificial data was given in this formula

$$\alpha(p) = \beta(p) - \beta(P) + \lambda(P) + \tau(\beta(1) - \beta(P)) \quad (7)$$

where $p = 1, 2, \dots, P$; β is the 95th percentile of singular values of the simulated data; and the parameter τ is constant.

For a given image patch size 5×5 pixels, Figs. 1 and 2 show the eigenimages, the singular values λ and α , and PA for the normalised 'camera' and 'house' images corrupted by the AWGN with zero mean and standard deviation $\sigma = 0.1$, respectively. The numbers of significant components of 'camera' and 'house' images are separately estimated as 16 and 9. The larger dimension number can be attributed to

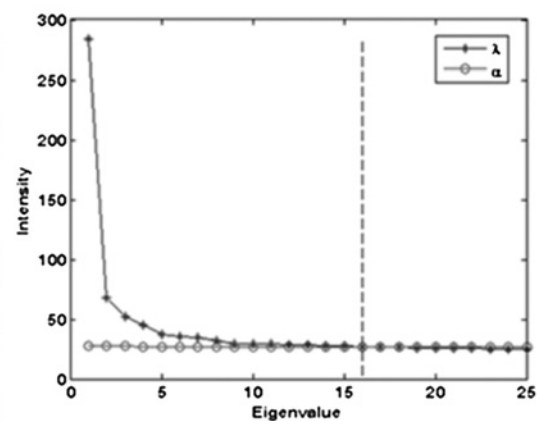
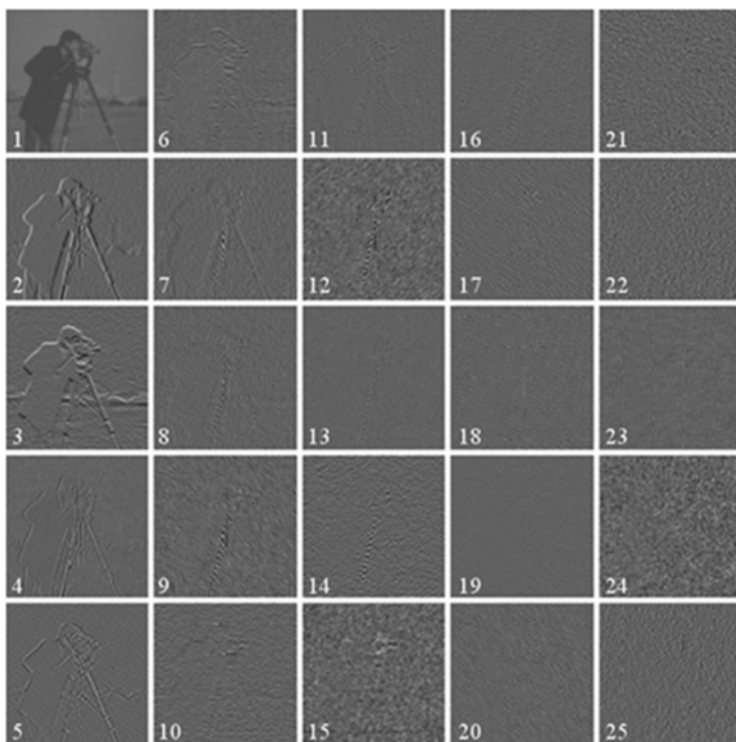


Fig. 1 Eigenimages, the singular values λ and α computed in this manner from the camera image

Left: the eigenimages from the 'camera' image, Right: two lines of the singular values by PA

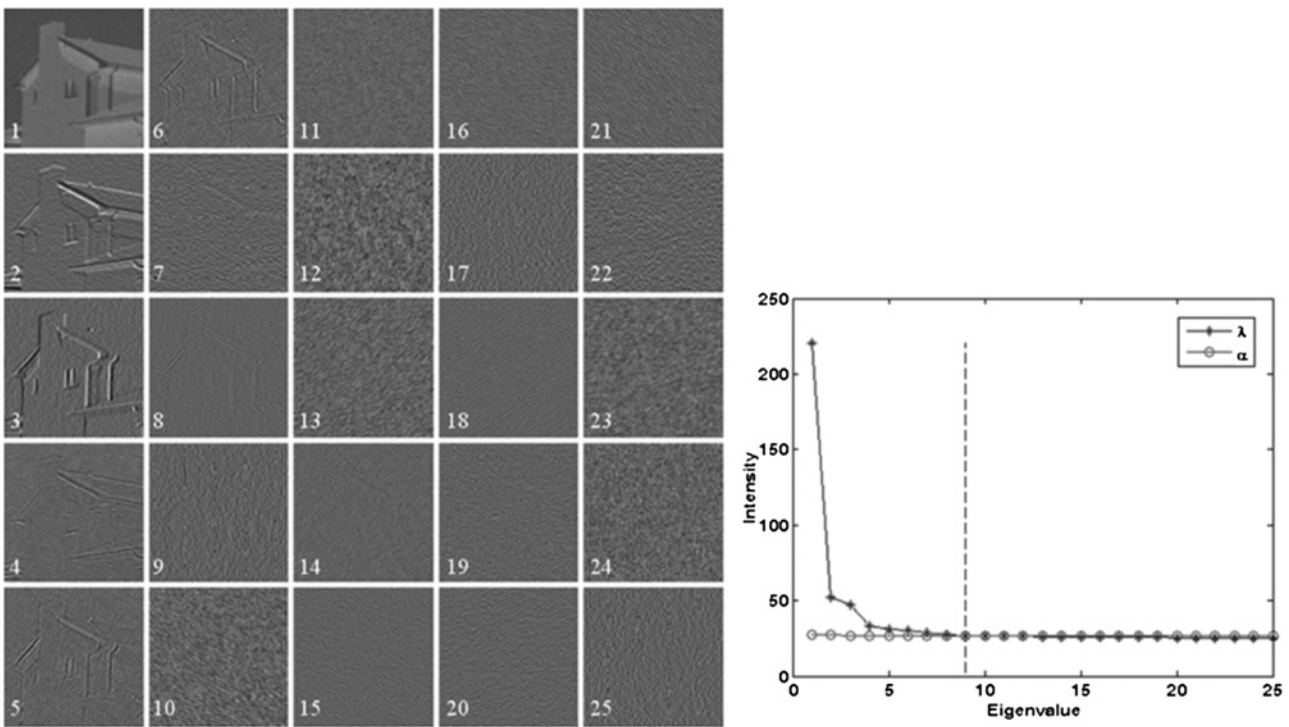


Fig. 2 Eigenimages, the singular values λ and α computed in this manner from the house image

Left: the eigenimages from the ‘house’ image, Right: two lines of the singular values by PA

the textured nature of the ‘camera’ image which verifies the robustness and effectiveness of the proposed approach. As can be seen, the improved PA method can automatically choose the threshold to separate signal and noise [35]. Note that when the number of factors $K=P$, the chosen eigenvalues by the proposed approach are equivalent to those of the original data.

2.4 Signal subspace projection

The eigenvectors of the generated vectorised patch-based matrix Z can be used for principal component analysis (PCA) of the noisy image X . Based on the observation that most of the energy of the clean image is concentrated at principal components whereas the eigenimages of the small singular values are almost all noises, we develop one novel denoising scheme based on projection onto the signal subspace spanned by the first K eigenvectors almost without loss of signal information. The M by N noisy image matrix X is converted into a column vector I of size $M \times N$ by 1 in this form

$$I((m-1)N+n) = x(m, n) \quad (8)$$

where $m = 1, 2, \dots, M$; and $n = 1, 2, \dots, N$.

The straightforward way to restore an image is to directly project the noisy image vector I onto the subspace spanned by the top K eigenvectors. The projected weight matrix on the signal subspace basis is

$$W_p = \hat{Z}_{i,p} \setminus I_i \quad (9)$$

where $p = 1, 2, \dots, P$, and \setminus denotes the matrix left division operator. After the top K weights are truncated by the

refined PA with Monte Carlo simulation, the projected reconstructed image based on weighted subspace basis is

$$R_i = \hat{Z}_{i,p} \times W_p + \frac{1}{L} \sum_{i=1}^L I_i \quad (10)$$

where $i = 1, 2, \dots, L$; and $p = 1, 2, \dots, K$. Then the reorganised reference image is reshaped as

$$R(m, n) = R_i((m-1)N+n) \quad (11)$$

where $m = 1, 2, \dots, M$; and $n = 1, 2, \dots, N$.

2.5 Proposed filtering approach

The guided filter [24] is to apply the filter kernel weights computed from guided image to the more noisy image. Specifically, the filtering output image f at a pixel i is computed as a weighted average of pixel neighbourhoods

$$f_i = \sum_j W_{ij} x_j \quad (12)$$

where i and j are pixel indexes, and a pixel i is involved in all the windows ω_k that contain i .

The filter kernel W_{ij} is a function of the guidance image I and independent of the noisy image X , and W_{ij} is normalised weight, viz. $\sum_j W_{ij}(I) = 1$. The kernel weights can be explicitly written by

$$W_{ij}(I) = \frac{1}{|\omega|^2} \sum_{k:(i,j) \in \omega_k} \left(1 + \frac{(I_i - \mu_k)(I_j - \mu_k)}{\sigma_k^2 + \varepsilon} \right) \quad (13)$$

where $|\omega|$ is the total number of pixels in a window ω_k ; μ_k and σ_k^2 are the mean and variance in a window ω_k of the guide image I ; and ε is a regularisation parameter.

In previous literatures [24, 30], the guided image I and input noisy image X are identical when the guided filter is used for single image denoising. However, the noise existing in guided image brings about distortion of the restored image, and also the parameter ε seriously affects the filtering results. To solve this problem, in the proposed algorithm, we select the reconstructed reference image R even though it still has some residual noise after signal subspace projection (SSP) as the guided image I , and simultaneously optimise the parameter ε under different window size by noise deviation estimation for noise reduction further.

For a given noisy image and a window ω_k of pixel neighbourhood, the optimal choice of the parameter ε in (13) yields the best output in terms of PSNR. After the reference image from (11) is taken as the guide image in the literature [24], the improved PCA guided filter and the traditional guided filter in [24] with various ε were compared in Fig. 3, which shows the PSNR of the estimator output f as a function of the parameter ε for ‘lena’ image corrupted with AWGN with zero mean and standard deviation $\sigma=0.10$. In this simulation, while the window size (5×5 pixels) is used for both of them, our reference image is reconstructed using the 10 largest singular values of patch-based image from an input noisy image with patch size (9×9 pixels). We used search procedures of gold standard to find the parameter value ε with the error less than 10^{-6} that maximises the output PSNR.

In Fig. 4, the optimal ε values of the proposed PCA guided filter and the traditional guided filter are shown as a function of noise deviation σ and 5×5 image neighbourhoods, respectively. The proposed PCA guided filter finds the guide image in the following way: it reconstructs the guide image from noisy image by projecting onto the corresponding eigenvectors of the 10 largest singular values. In our experiments, the eight test images selected from the USC-SIPI Image database [36] are shown in Fig. 5. Five of them, that is, ‘Lena’, ‘house’, ‘Barbara’, ‘camera’ and ‘aerial’, were corrupted with variant noise deviation $\sigma=0.04, 0.07, 0.10, 0.12, 0.14$ were used to

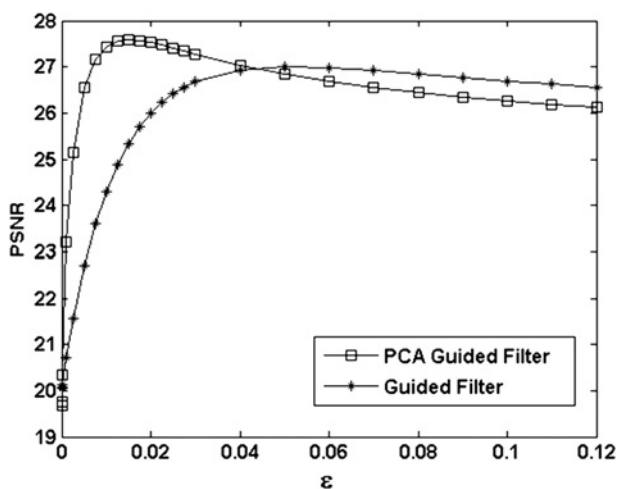


Fig. 3 Comparison of PSNR (dB) as a function of the parameter ε for improved PCA guided filter and the traditional guided filter individually applied on the normalised noisy lena image

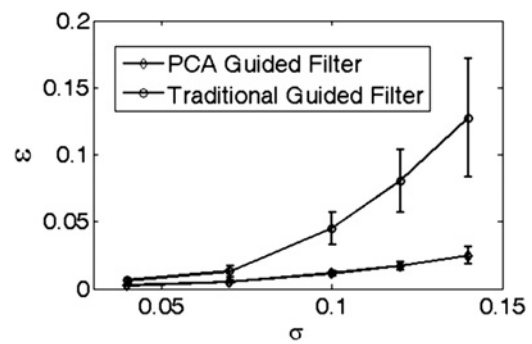


Fig. 4 Suboptimal parameter ε value as a function of noise deviation σ

verify the relationship between optimal parameter ε and noise deviation σ . The optimal value of ε behaves in a very predictable way with the use of noise deviation σ . As can be seen, for a fixed window size, for example, 5×5 pixels, the relationship between optimal ε and σ is approximately quadratic relation for both the proposed PCA guided filter and the traditional guided filter using variant test images, but the coefficients of quadratic functions are different. Therefore, under the given $r \times r$ image neighbourhoods and the dimensionality K of factors for noisy images, we utilise the quadratic fit to estimate the parameter ε as a function of noise deviation σ .

$$\varepsilon = a_2\sigma^2 + a_1\sigma + a_0 \quad (14)$$

Muresan and Parks [34] employed the smallest singular value of sample image neighbourhoods to estimate noise deviation with quite small bias error, that is, $\hat{\sigma} = \lambda_p/255$. Therefore this noise estimate technique can be used together with (14) to automatically select a suboptimal parameter ε value under the given image neighbourhood size $r \times r$ and dimensionality of factors K for a single noisy image. Through five training images, Table 1 illustrates the quadratic fit parameters of the proposed PCA guided filter for the chosen dimensionality $K=10$ of factors in the patch-based noisy images with block size 9×9 pixels, and also shows the quadratic fitting error and resulting loss of PSNR in the denoised image. It can be seen that the PSNR loss resulting from using the automatic parameter ε selection in substitution for the optimal ε is negligible because of the smooth broad maximum PSNR output curves shown in Fig. 3. Therefore, the robust estimation of the parameter ε is to take much larger set of training images to select it by these quadratic fits. The same analysis approach can be applied to other patch size and denoising algorithms. As we know, the suboptimal parameter ε also depends on the neighbourhood size. However, this automatic selection problem of the optimal neighbourhood window ω_k with the size $r \times r$ is difficult to solve, which is our future work to be done.

2.6 Image quality metrics

To perform a quantitative comparison between the performances of the different denoising algorithms, we computed some well-known noise-reduction full reference quality metrics [37–39]. The first measure criterion is the PSNR, defined by (15), where $I(x, y)$ denotes the samples of the normalised original image, $\hat{I}(x, y)$ denotes the



Fig. 5 Test images used in the experiments: *Lena, House, Barbara, Camera, Aerial, Airplane, Clock, and Chemical plant*

Table 1 Curve-fitting coefficients used for determining ε under signal subspace dimensionality of 9×9 image patch with L2 error in fit to optimal ε where there is about 0.05 dB loss in output PSNR

Coefficients	a_2	a_1	A_0	L2 error
$K = 10$	1.8922	-0.1188	0.0043	0.0169

samples of the filtered image. And M and N are the number of pixels in row and column directions, respectively.

$$\text{PSNR} = 10 \log_{10} \frac{1}{(1/MN) \sum_x \sum_y |I(x, y) - \hat{I}(x, y)|^2} \quad (15)$$

Another criterion is the structural similarity (SSIM) index for measuring the similarity between two images, which is designed to improve on the traditional methods like PSNR and MSE, which have proved to be inconsistent with human eye perception. The SSIM metric between two images x and y of common size $M \times N$ is calculated as

$$\text{SSIM}(x, y) = \frac{(2\mu_x\mu_y + c_1)(2\sigma_{xy} + c_2)}{(\mu_x^2 + \mu_y^2 + c_1)(\sigma_x^2 + \sigma_y^2 + c_2)} \quad (16)$$

Table 2 PCA-based signal subspace dimensionality selected by the refined PA with Monte Carlo simulation

Patch size (pixels)	3×3			5×5			7×7			9×9		
noise deviation	0.04	0.10	0.14	0.04	0.10	0.14	0.04	0.10	0.14	0.04	0.10	0.14
Lena	8	5	4	15	10	8	23	15	9	33	19	14
house	7	6	3	18	8	7	28	14	12	41	23	15
Barbara	7	6	6	17	12	7	14	10	7	18	12	9
camera	8	7	7	21	17	16	41	33	17	65	50	26
aerial	8	8	7	21	15	13	30	21	15	39	29	21
airplane	5	4	3	8	7	5	14	11	8	20	13	11
clock	7	6	6	16	11	10	33	18	13	43	25	19
plant	7	7	6	14	10	8	25	13	13	35	20	16

where μ_x denotes the average of the image x ; μ_y denotes the average of the image y ; σ_x^2 is the variance of the image x ; σ_y^2 is the variance of the image y ; σ_{xy} is the covariance of x and y ; the two variables $c_1 = (k_1L)^2$ and $c_2 = (k_2L)^2$ stabilise the division with weak denominator where L represents the dynamic range of the pixel-values, and $k_1 = 0.01$ and $k_2 = 0.03$ by default. The resultant SSIM index is a decimal value between 0 and 1, and value 1 is only reachable in the case of two identical sets of data.

3 Results and analysis

3.1 Dimensionality of signal subspace

A numerical simulation was designed for the proposed SSP-based denoising algorithm to determine the dimensionality of signal subspace under different image patch size. The numerical model with additive independent Gaussian noises with zero mean value and noise deviation $\sigma = 0.04, 0.10, 0.14$ individually was constructed according to (2). The improved PA with Monte Carlo simulation was used to choose the dimensionality of signal subspace in the vectorised patch-based noisy image formulated from the series of image patches centered at each pixel, and Table 2 shows the results of dimensionality selected from the eight test images. It can be seen that the dimensionality of signal subspace in noisy image decreases when noise level increases. Furthermore, it is conducive to distinguish

Table 3 PSNR and SSIM results for images denoised by the proposed algorithm with image patch size 9×9 pixels, and the traditional guided filter [24]

Deviation σ	5×5 Proposed	5×5 [24]	7×7 Proposed	7×7 [24]	9×9 Proposed	9×9 [24]
Lena	31.86/0.875	31.35/0.845	31.27/0.858	30.87/0.831	30.85/0.844	30.53/0.819
	27.23/0.737	24.47/0.536	26.51/0.706	24.24/0.521	25.64/0.641	24.00/0.507
	25.88/0.673	22.43/0.432	25.20/0.642	22.27/0.416	24.58/0.609	22.07/0.403
house	33.22/0.859	32.33/0.810	32.81/0.853	32.05/0.806	32.47/0.844	31.79/0.798
	28.01/0.680	24.82/0.452	27.53/0.668	24.69/0.444	27.05/0.649	24.52/0.435
	26.78/0.638	22.64/0.351	26.30/0.631	22.57/0.342	25.75/0.611	22.42/0.334
Barbara	31.11/0.879	30.84/0.861	30.68/0.867	30.40/0.847	30.27/0.852	30.01/0.833
	26.51/0.750	24.21/0.584	25.81/0.717	23.92/0.566	25.16/0.680	23.61/0.549
	25.17/0.695	22.17/0.480	24.45/0.662	21.96/0.463	23.76/0.622	21.69/0.447
camera	32.03/0.859	31.82/0.844	31.77/0.855	31.59/0.839	31.53/0.848	31.37/0.833
	25.66/0.604	24.49/0.517	25.48/0.599	24.36/0.510	25.18/0.582	24.19/0.501
	23.86/0.528	22.12/0.412	23.77/0.534	22.02/0.404	23.34/0.503	21.87/0.395
aerial	29.52/0.913	29.44/0.909	29.09/0.903	29.05/0.900	28.83/0.895	28.81/0.893
	24.06/0.754	23.12/0.706	23.35/0.718	22.73/0.685	22.90/0.695	22.44/0.671
	22.58/0.678	21.20/0.607	21.85/0.635	20.84/0.583	21.32/0.605	20.54/0.566
airplane	36.10/0.923	33.56/0.797	35.69/0.920	33.40/0.796	35.18/0.911	33.15/0.789
	29.97/0.768	25.35/0.382	29.72/0.774	25.35/0.379	29.29/0.761	25.26/0.374
	28.17/0.728	23.12/0.289	27.98/0.749	23.17/0.288	27.59/0.739	23.12/0.283
clock	33.09/0.889	32.33/0.835	32.67/0.884	32.01/0.829	32.32/0.875	31.74/0.822
	27.02/0.694	24.91/0.494	26.60/0.682	24.76/0.487	26.27/0.671	24.60/0.479
	25.31/0.647	22.74/0.403	25.22/0.696	22.64/0.396	24.55/0.627	22.50/0.389
plant	30.40/0.868	30.19/0.860	29.98/0.856	29.85/0.850	29.72/0.849	29.61/0.843
	25.56/0.700	23.82/0.598	24.97/0.667	23.58/0.581	24.55/0.645	23.38/0.570
	24.41/0.643	21.84/0.490	23.68/0.594	21.67/0.472	23.28/0.576	21.49/0.461

For each image, the 3 rows correspond to the noise deviation $\sigma = 0.04, 0.10$ and 0.14 , respectively

Table 4 PSNR and SSIM results for images denoised by the proposed algorithm with image patch size 9×9 pixels, and the bilateral filter [21]

Deviation σ	5×5 Proposed	5×5 [21]	7×7 Proposed	7×7 [21]	9×9 Proposed	9×9 [21]
Lena	31.86/0.875	30.37/0.804	31.27/0.858	30.40/0.804	30.85/0.844	30.37/0.802
	27.23/0.737	23.77/0.512	26.51/0.706	23.89/0.513	25.64/0.641	23.89/0.509
	25.88/0.673	21.40/0.401	25.20/0.642	21.58/0.400	24.58/0.609	21.60/0.396
house	33.22/0.859	31.10/0.748	32.81/0.853	31.30/0.758	32.47/0.844	31.33/0.759
	28.01/0.680	24.01/0.421	27.53/0.668	24.25/0.430	27.05/0.649	24.31/0.429
	26.78/0.638	21.47/0.315	26.30/0.631	21.73/0.320	25.75/0.611	21.80/0.318
Barbara	31.11/0.879	30.10/0.831	30.68/0.867	30.13/0.831	30.27/0.852	30.10/0.829
	26.51/0.750	23.54/0.560	25.81/0.717	23.63/0.561	25.16/0.680	23.61/0.557
	25.17/0.695	21.21/0.448	24.45/0.662	21.34/0.447	23.76/0.622	21.34/0.443
camera	32.03/0.859	30.94/0.781	31.77/0.855	31.10/0.788	31.53/0.848	31.15/0.790
	25.66/0.604	24.07/0.495	25.48/0.599	24.30/0.503	25.18/0.582	24.37/0.504
	23.86/0.528	21.51/0.390	23.77/0.534	21.75/0.396	23.34/0.503	21.87/0.396
aerial	29.52/0.913	29.29/0.905	29.09/0.903	29.28/0.904	28.83/0.895	29.25/0.903
	24.06/0.754	22.77/0.701	23.35/0.718	22.75/0.695	22.90/0.695	22.68/0.690
	22.58/0.678	20.53/0.593	21.85/0.635	20.54/0.585	21.32/0.605	20.47/0.578
airplane	36.10/0.923	31.83/0.701	35.69/0.920	32.11/0.713	35.18/0.911	32.22/0.717
	29.97/0.768	24.65/0.349	29.72/0.774	24.97/0.360	29.29/0.761	25.08/0.363
	28.17/0.728	22.26/0.256	27.98/0.749	22.58/0.265	27.59/0.739	22.70/0.266
clock	33.09/0.889	31.26/0.757	32.67/0.884	31.43/0.766	32.32/0.875	31.47/0.768
	27.02/0.694	24.46/0.469	26.60/0.682	24.66/0.478	26.27/0.671	24.71/0.479
	25.31/0.647	22.20/0.379	25.22/0.696	22.42/0.386	24.55/0.627	22.47/0.386
plant	30.40/0.868	29.69/0.846	29.98/0.856	29.68/0.844	29.72/0.849	29.65/0.843
	25.56/0.700	23.28/0.586	24.97/0.667	23.33/0.580	24.55/0.645	23.31/0.576
	24.41/0.643	20.97/0.469	23.68/0.594	21.08/0.462	23.28/0.576	21.09/0.457

For each image, the three rows correspond to the noise deviation $\sigma = 0.04, 0.10$ and 0.14 , respectively

between signal and noise for the eigenimages with fine-scale structures when the patch size increases.

3.2 Implementation and experiments

Several experiments using multiple test images have been done to verify the performance of our proposed algorithm. The eight selected test images including 'airplane', 'clock', 'Chemical plant' and previous five training images used for our experiments are a subset of the

USC-SIPI image database [36]. The original images were added with AWGN with different variance, for both the subjective evaluation and the objective evaluation of the denoising performance between the proposed SSP-based algorithm and the state of the arts [21, 24, 25]. Moreover, for different types of test images, numerous experiments for noise reduction have been implemented and the results were compared to verify the validity and the robustness of the proposed algorithm.

Table 5 Comparison for the computation time between the proposed algorithm and the denoising methods in [21, 24], respectively

Methods	[24]	[21]	Proposed
time, s	0.25	1.52	1.63

Experiments are performed on well-known 8-bit grey-scale test images. We compared our work based on PSNR and SSIM, which is a method for measuring the similarity between two images (the original and the processed images) reportedly assessing image qualities more reliably than PSNR [39]. In this experiment, the test images were degraded by additive Gaussian noise with zero means and different deviations $\sigma=0.04, 0.10$ and 0.14 , respectively. The performances of our developing algorithm were

compared with the state-of-the-art denoising methods published recently [21, 24, 25]. The PSNR and SSIM results for test images under different neighbourhood windows (e.g. 5×5 , 7×7 and 9×9 pixels) are shown in Tables 3 and 4. Here the image patch size used in the proposed algorithm is 9×9 pixels, which is also the same with that of the traditional guided filter [24] for a fair comparison. The spatial-domain and the intensity-domain deviation of the bilateral filter [21] are 3 and σ , respectively. Moreover, Table 5 demonstrates that the proposed algorithm and the methods in the literatures [21, 24] were compared in computation time using Matlab version 7.8 on the platform of Pentium(R) Dual-Core CPU E5800 @3.20 GHz 2 GB cache for 256×256 test images, respectively. Compared with the state-of-the-art methods, the proposed algorithm can greatly improve filtering results with loss of a little increase in computational time. Fig. 6

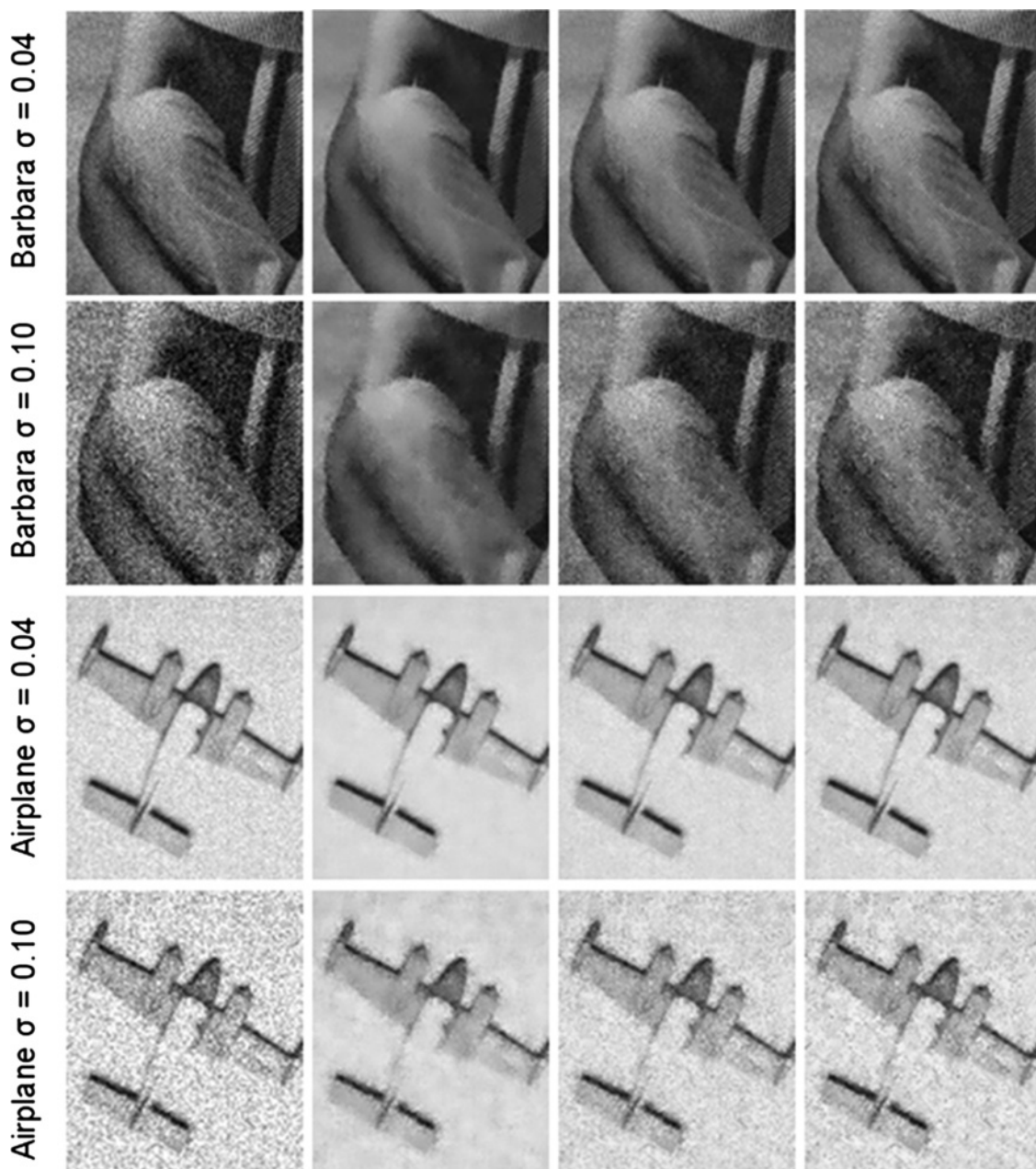


Fig. 6 Visual comparison of the noisy images, the proposed algorithm, the traditional guided filter [24], and the bilateral filter [21] using the same image neighbourhoods 5×5 pixels

shows the detailed results of noise removal for the proposed method, the traditional guided filter [24], and the bilateral filter [21] for the fragments of the normalised 'Barbara' and 'Airplane' images. As seen from the experimental results, the proposed algorithm, which can reach better results than the state-of-the-art methods on noise removal, works well for a wide variety of noisy images, and can remove more noise, restore clearer images, preserve more details and sharper edges.

4 Conclusion and future work

In this paper, we presented a novel denoising algorithm which is based on the guided filter. The reference image of the proposed algorithm is reconstructed from the noisy image projected onto the lower-dimensional signal subspace based on global PCA determined by refined parallel analysis with Monte Carlo simulation for the high-dimensional patch-based noisy image matrix. We have addressed the problem of determining the dimensionality of the signal subspace in the noisy image under certain image patch size and the automatic selection of the optimal parameters of the guided image filter. The smallest singular value of the patch-based image matrix by SVD is used to estimate image noise deviation, which is adopted to automatically choose the optimal parameter value of the improved guided filter algorithm. The relationship between noise deviation and the optimal parameter value can be established by fitting polynomial model through pre-computing the output maximum PSNR of test image corrupted with different noise level. Although the proposed algorithm is generalisation of the guided image filter with small loss of computational efficiency, it was observed that our SSP-based denoising algorithm performs much better than the traditional guided image filter and other state-of-the-arts methods both visually and quantitatively. Moreover, the reconstructed image from the lower-dimensional projections using the improved PA approach with Monte Carlo simulations can also be easily applied on other denoising and filtering algorithms for weight function calculation. Finally, the automatic selection of the optimal image neighbourhood size of the denoising algorithm and the further reduction of computation time are left for our future research.

5 Acknowledgments

This work was supported by National Basic Research Program (973 Program) of China under Contract No. 2009CB320907, National Natural Science Foundation of China under contract No. 61101078, and Doctoral Fund of Ministry of Education of China under contract No. 20110001120117. The authors would like to thank the editors and reviewers gratefully for their efforts, comments, and recommendations, which have led to a substantial improvement of the technical content and the presentation quality of this manuscript.

6 References

- Nahi, N.E.: 'Role of recursive estimation in statistical image enhancement', *Proc. IEEE*, 1972, **60**, (7), pp. 872–877
- Lev, A., Zucker, S.W., Rosenfeld, A.: 'Iterative enhancement of noisy images', *IEEE Trans. Syst., Man Cybern.*, 1977, **7**, (6), pp. 435–442
- Lee, J.S.: 'Digital image enhancement and noise filtering by use of local statistics', *IEEE Trans. Pattern Anal. Mach. Intell.*, 1980, **2**, (2), pp. 165–168
- Donoho, D.L.: 'De-noising by soft-thresholding', *IEEE Trans. Inf. Theory*, 1995, **41**, (3), pp. 613–627
- Simoncelli, E.P., Adelson, E.H.: 'Noise removal via Bayesian wavelet coining'. Proc. of Third IEEE Int. Conf. on Image Processing, September 1996, pp. 379–382
- Mihcak, M.K., Kozintsev, I., Ramchandran, K., Moulin, P.: 'Low complexity image denoising based on statistical modeling of wavelet coefficients', *IEEE Signal Process. Lett.*, 1999, **6**, (12), pp. 300–303
- Li, X., Orchard, M.: 'Spatially adaptive image denoising under overcomplete expansion', *Int. Conf. on Image Processing (ICIP)*, 2000, **3**, pp. 300–303
- Chang, S.G., Yu, B., Vetterli, M.: 'Adaptive wavelet thresholding for image denoising and compression', *IEEE Trans. Image Process.*, 2000, **9**, (9), pp. 1532–1546
- Starck, J.L., Cands, E.J., Donoho, D.L.: 'The curvelet transform for image denoising', *IEEE Trans. Image Process.*, 2002, **11**, (6), pp. 670–684
- Portilla, J., Strela, V., Wainwright, M.J., Simoncelli, E.P.: 'Image denoising using scale mixtures of gaussians in the wavelet domain', *IEEE Trans. Image Process.*, 2003, **12**, (11), pp. 1338–1351
- Bhutada, G.G., Anand, R.S., Saxena, S.C.: 'Image enhancement by wavelet-based thresholding neural network with adaptive learning rate', *IET Image Process.*, 2011, **5**, (7), pp. 573–582
- Buades, A., Coll, B., Morel, J.M.: 'A review of image denoising algorithms, with a new one', *Multiscale Model. Simul.*, 2005, **4**, (2), pp. 490–530
- Tasdizen, T.: 'Principal neighborhood dictionaries for non-local means image denoising', *IEEE Trans. Image Process.*, 2009, **18**, (12), pp. 2649–2260
- Weissman, T., Ordentlich, E., Seroussi, G., Verd, S., Weinberger, M.: 'Universal discrete denoising: Known channel', *IEEE Trans. Inf. Theory*, 2005, **51**, (1), pp. 5–28
- Awate, S.P., Whitaker, R.T.: 'Unsupervised, information-theoretic, adaptive image filtering for image restoration', *IEEE Trans. Pattern Anal. Mach. Intell.*, 2006, **28**, (3), pp. 364–376
- Aharon, M., Elad, M., Bruckstein, A.M.: 'K-SVD: An algorithm for designing of overcomplete dictionaries for sparse representation', *IEEE Trans. Signal Process.*, 2006, **54**, (11), pp. 4311–4322
- Elad, M., Aharon, M.: 'Image denoising via sparse and redundant representations over learned dictionaries', *IEEE Trans. Image Process.*, 2006, **15**, (12), pp. 3736–3745
- Hirakawa, K., Parks, T.W.: 'Image denoising using total least squares', *IEEE Trans. Image Process.*, 2006, **15**, (9), pp. 2730–2742
- Foi, A., Katkovnik, V., Egiazarian, K.: 'Pointwise shape-adaptive DCT for high-quality denoising and deblocking of grayscale and color images', *IEEE Trans. Image Process.*, 2007, **16**, (5), pp. 1395–1411
- Dabov, K., Foi, A., Katkovnik, V., Egiazarian, K.: 'Image denoising by sparse 3D transform-domain collaborative filtering', *IEEE Trans. Image Process.*, 2007, **16**, (8), pp. 2080–2095
- Tomasi, C., Manduchi, R.: 'Bilateral filtering for gray and color images'. Proc. of the Sixth Int. Conf. on Computer Vision, 1998, pp. 839–846
- Takeda, H., Farsiu, S., Milanfar, P.: 'Kernel regression for image processing and reconstruction', *IEEE Trans. Image Process.*, 2007, **16**, (2), pp. 349–366
- Zhang, Y., Ai, Y., Dai, K., Zhang, G.: 'Grey model via polynomial for image denoising', *J. Grey Syst.*, 2010, **22**, (2), pp. 117–128
- He, K., Sun, J., Tang, X.: 'Guided image filtering', *Comput. Vis. – ECCV 2010, Lect. Notes Comput. Sci.*, 2010, **6311**, pp. 1–14
- Rydell, J., Knutsson, H., Borga, M.: 'Bilateral filtering of fMRI data', *IEEE J. Sel. Top. Signal Process.*, 2008, **2**, (6), pp. 891–896
- Ding, Y., Chung, Y.C., Simonetti, O.P.: 'A method to assess spatially variant noise in dynamic MR image series', *Magn. Reson. Med.*, 2010, **63**, (3), pp. 782–789
- Park, S.W., Kang, M.G.: 'Image denoising filter based on patch-based difference refinement', *Opt. Eng.*, 2012, **51**, (6), pp. 067007:1–13
- Chul, L., Chulwoo, L., Chang-Su, K.: 'An MMSE approach to nonlocal image denoising: Theory and practical implementation', *J. Vis. Commun. Image Represent.*, 2012, **23**, (3), pp. 476–490
- Zhang, L., Li, X., Zhang, D.: 'Image denoising and zooming under the linear minimum mean square-error estimation framework', *IET Image Process.*, 2012, **6**, (3), pp. 273–283
- Pablo, B., Martin, E., Marcus, M.: 'Guided image filtering for interactive high-quality global illumination', *Comput. Graph. Forum*, 2011, **30**, (4), pp. 1361–1368
- Xiao, C., Gan, J.: 'Fast image Dehazing using guided joint bilateral filter', *Vis. Comput.*, 2012, **28**, (6–8), pp. 713–721

- 32 Horn, J.L.: 'A rationale and test for the number of factors in factor analysis', *Psychometrika*, 1965, **30**, (2), pp. 179–185
- 33 Jorgensen, K.W., Hansen, L.K.: 'Model selection for Gaussian kernel PCA denoising', *IEEE Trans. Neural Netw. Learn. Syst.*, 2012, **23**, (1), pp. 163–168
- 34 Muresan, D.D., Parks, T.W.: 'Adaptive principal components and image denoising', *IEEE Int. Conf. Image Process. (ICIP)*, 2003, **1**, pp. 101–104
- 35 Azzabou, N., Paragios, N., Guichard, F.: 'Image denoising based on adapted dictionary computation', *IEEE Int. Conf. Image Process. (ICIP)*, 2007, **3**, pp. III-109–III-112
- 36 Weber, A.: 'The USC-SIPI image database', June 1, 2012, available at <http://www.sipi.usc.edu/database/>
- 37 Chikkerur, S., Sundaram, V., Reisslein, M., Karam, L.J.: 'Objective video quality assessment methods: a classification, review, and performance comparison', *IEEE Trans. Broadcast.*, 2011, **57**, (2), pp. 165–182
- 38 Huynh-Thu, Q., Ghanbari, M.: 'Scope of validity of PSNR in image/video quality assessment', *Electron. Lett.*, 2008, **44**, (13), pp. 800–801
- 39 Wang, Z., Bovik, A.C., Sheikh, H.R., *et al.*: 'Image quality assessment: from error visibility to structural similarity', *IEEE Trans. Image Process.*, 2004, **13**, (4), pp. 600–612